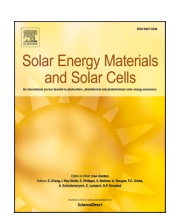
FISEVIER

Contents lists available at ScienceDirect

Solar Energy Materials and Solar Cells

journal homepage: www.elsevier.com/locate/solmat





Blade-coated inverted perovskite solar cells in an ambient environment

Xinwen Zhang ^a, Lening Shen ^b, Pramod Baral ^a, S.N. Vijayaraghavan ^c, Feng Yan ^c, Xiong Gong ^{b,**}, He Wang ^{a,*}

- ^a Department of Physics, University of Miami, Coral Gables, FL, 33146, USA
- b School of Polymer Science and Polymer Engineering, College of Engineering and Polymer Science, The University of Akron, Akron, OH, 44325, USA
- ^c Department of Metallurgical and Materials Engineering, The University of Alabama, Tuscaloosa, AL, 35487, USA

ARTICLE INFO

Keywords: Perovskite solar cells Blade coating Vacuum quenching Ambient environment

ABSTRACT

To make the jump from laboratories to commercial production for perovskite solar cells, it is necessary to develop devices in an ambient environment using materials and methods that can be scalable. Here, blade coating followed by vacuum quenching is used to manufacture the FACs-based perovskite solar cells with the additive of MACl under an ambient environment (30%–57% RH), where FA is formamidinium and MA is methylammonium. The vacuum allows quick removal of solvent to initiate the nucleation process and create the intermediate phase. To control the nucleation and crystallization, the additive MACl is utilized to manipulate the intermediate phase. Besides perovskites, another key component is the hole transport material. Although nickel oxide exhibits good photostability and can be scalable for the inverted device architecture, the main drawback is low cell efficiency. This work solves it by tuning the cation ratio of Pb^{2+} to A^+ and light soaking, achieving a champion efficiency of 19.5%. The encapsulated solar cells exhibit long-term photostability, maintaining 96% of their original efficiency and 91.5% of their maximum efficiency over 648 h under one sun at 45° C and 50%–60% relative humidity. This work demonstrates an economical and highly scalable process, promising for commercial-scale manufacturing.

1. Introduction

Perovskite solar cells (PSC) have developed at a breakneck pace in the last decade, reaching the power conversion efficiency (PCE) of 25.7% [1]. Such high PCE of PSCs is due to several properties, such as strong absorption in the visible range, the long diffusion length of charge carriers, and defect tolerance of hybrid inorganic-organic perovskites [2–4]. To make the jump from laboratories to commercial production, it is necessary to develop low-cost large-area devices in an ambient environment. Traditional lab-scale fabrication methods, such as spin coating in a nitrogen environment, are ill-suited for large-area manufacturing processes. Many scalable techniques [5–9] were developed, among which slot die [10–13] and blade coating [14–21] are attractive, as they consistently achieve uniformity over large areas with high yield. Since slot die wastes the first few mL of perovskite precursor in the slot die head, a similar approach, namely blade coating, which wastes a negligible amount, is typically applied at the beginning to optimize the ink.

A crucial challenge for blading uniform and mirror-like perovskite

films is the nucleation and crystallization process. The literature and general understanding of the crystallization process on blade coating for cells and modules are much less than those on spin coating. Many factors such as precursor solvent [22], temperature [23], humidity [24], and solvent evaporation rate [25,26], all affect the nucleation and crystallization process [27]. A further hurdle is that knowledge of nucleation and crystallization using spin coating does not fully apply to blade coating [28]. For example, dimethylformamide (DMF), dimethyl sulfoxide (DMSO), and their mixtures are typically used during spin coating. But it is not straightforward to control their evaporation during blade coating, in particular for FACs-based perovskite in air, where MA is methylammonium. For better thermal stability, MA⁺ is substituted by FA⁺ (formamidinium), which has lower volatility, or a mixture of FA⁺ and Cs⁺. Compared with MA ink, FACs ink is more difficult to develop, since FAPbI₃ favors the yellow phase at room temperature, especially in air [29]. To bridge this gap, in this study, we use solvent N-methyl-2-pyrrolidone (NMP) to replace the conventional co-solvent DMSO to fabricate perovskite film under ambient environment. Compared with

E-mail addresses: xgong@uakron.edu (X. Gong), hewang@miami.edu (H. Wang).

^{*} Corresponding author.

^{**} Corresponding author.

DMSO, NMP has a stronger interaction with FA, which can facilitate the formation of a more stable FAI•PbI₂•NMP [10,30–32]. Furthermore, NMP has lower vapor pressure compared with DMSO, which can slow the crystallization speed, leading to a dense and uniform perovskite film. Although NMP is not a "green" solvent, only a small amount of precursor is needed: 5 μ L for a 2×2 cm² substrate and 10 μ L for a 5×5 cm².

Moreover, antisolvent used to quickly extract the solvent during the spin coating process is limited to small areas, making it highly unsuited for large-scale manufacturing. Another drawback in the spin coating is that the nucleation process, crucial to fabricate efficient PSCs, occurs over only a few seconds, and is sensitive to the time when the antisolvent is added, greatly hampering its reproducibility. One alternative consists in using an air knife [33,34], applied to blade coating, to bring the precursor to the intermediate phase in a few seconds. This approach is very efficient for easily vaporized solvents. But as our solvents, e.g., NMP, are not easily vaporized, we use the vacuum assistant method [35] to easily extract it from the wetting substrates. To upscale the vacuum quenching in industry, since the pressure needs to be uniform, the air can be easily extracted by uniformly distributed holes.

To fabricate high-quality film with larger grains and fewer grain boundaries, thus improving PCE, several other methods, such as interface engineering [36], compositional engineering [37], and additive engineering [38], can be employed. Among these methods, a chlorinated molecule is a commonly used additive to improve the film morphology of perovskite. It has been widely reported that MACl is a good additive to increase the crystallization of α -phase by forming an intermediate phase, which inhibits the formation of δ -phase of perovskite [39–41]. In our experiment, we found that MACl can also promote the formation of more intermediate phases in the vacuum quenching process. We observed that MACl alters the color of the film, after the vacuum assistant method, making it more of a darker shade of brown, while the film without MACl is of yellowish-brown color.

Besides the perovskite film, another key component is the substrate. The premier choice has been the organic hole transport layer (HTL) poly (PTAA), [bis(4-phenyl)(2,4,6-trimethylphenyl)amine commonly used in the PSCs with the p-i-n device architecture, since the PSCs incorporated with the PTAA HTL could produce high PCE and negligible hysteresis. PTAA is, however, hydrophobic, which limits the choice of solvents. In particular, NMP is quite ill-suited for using over PTAA, as it cannot be uniformly spread after deposition. Therefore, we use an inorganic semiconductor NiOx as the HTL. It has lots of benefits, such as low cost, high photostability especially under the full light spectrum, hydrophilic surface, and scalability, making it as one of the best hole transport candidates for upscaling PSCs [42]. Many fabrication methods have been reported for NiOx, such as spin coating [43,44], hot spray [45], atomic layer deposition [46], and sputtering [47]. Among these techniques, atomic layer deposition, sputtering, and hot spray are all highly scalable, with the last one being our choice in this work. The main drawback of NiOx is the relatively low open-circuit voltage (Voc) caused by the interface defects and traps [48]. Also, the low conductivity of NiOx impedes the performance of PSCs. There are a plethora of methods to optimize NiOx, such as using Zn/Li/Mg/as a dopant to improve its conductivity and the work function [45,49,50], and alkali chloride (NaCl/KCl) to reduce defect/trap density and suppress the interfacial recombination [51]. Based on the physical properties of NiOx, in this work, we optimize by fine-tuning the ratio between Pb²⁺ and A⁺ cation to improve the PCE of PSCs. It has been reported that adding a slightly excessive amount of A⁺ cation can compensate iodide vacancies and suppress counterion migration and defect generation during the long-term illumination [52]. McGehee's group reported that $Ni^{\geq 3}$ sites in NiO_x thin film can react with AX, forming excess PbI₂ at the interface between perovskite and the NiOx HTL. The produced PbI2 at the interface will act as a hole extraction barrier, reducing device VOC [53]. Here, we decrease the amount of PbI₂ in perovskite precursors to enhance perovskite crystallinity, which improves the V_{OC} of PSCs. Moreover, using femtosecond laser transient absorption and reflection

spectroscopy, we find that light soaking can increase the carrier lifetime at the NiOx/perovskite interface, which also improves the $V_{\rm OC}$ of PSCs.

Our work combined the above methods to create an economical, easily controlled, and highly scalable process well-suited for commercial-scale manufacturing. First, since at this scale depositing perovskite layer occurs in air, as it is unfeasible to require a large nitrogen environment, a suitable solvent is needed. We solve this by using NMP to lower the formation energy of α phase perovskite in air. Removing this solvent at a commercial scale, however, cannot be feasibly done using classical methods such as antisolvent: we opt for the vacuum-assisted method. To control the nucleation and crystallization during vacuum, we use the additive MACl to produce an intermediate phase. Finally, for a process to be scalable, the substrate must be scalable too. PTAA is the current go-to choice, but its hydrophobic nature makes it hardly useable with NMP. An alternative is needed, and NiOx is our premier choice. The only drawback is that PSCs exhibit low PCEs, which we solve by fine-tuning the ratio of Pb²⁺ to A⁺ cations and light soaking. Therefore, this entire process, which focuses on being economical and highly scalable, is promising for making the leap from laboratories to commercial plants.

2. Results and discussion

2.1. The impact of additive MACl on the intermediate phase and device performance

Fig. 1a displays the schematic illustration of blade coating, intermediate phase after vacuum-assisted method, and perovskite thin-film after thermal annealing. The additive MACl in the perovskite precursor is utilized to increase the crystallization of α-phase by manipulating the intermediate phase (FAI·PbI₂·MACl) with the vacuum-assisted method. Thermal annealing at 150°C completely removes MACl from the film. Fig. 1b (i-iii) displays the photos of intermediate phase of FA_{0.8}Cs_{0.2}PbI₃ with different amount of MACl (0%, 4%, 10% molar ratio relative to Pb) after vacuum quenching. We can see they exhibit different colors. The film without MACl shows a light-yellow brown color, while the film with 4% MACl exhibits dark brown. Further increasing the amount of MACl to 10% results in an even darker film. The darker color represents that a more intermediate phase is produced during the vacuum quenching process. Fig. 1b (iv) displays perovskite films fabricated on substrates of two different sizes 2×2 cm² and 5×5 cm², proving that this method of blade coating and vacuum-assisted method can apply for large-area perovskite solar cell fabrication. The scanning electron microscopy (SEM) images of perovskite films with different amount of MACl were compared (Fig. 1 c-e). The film prepared with 4% MACl exhibits significant larger grain size and fewer grain boundaries. Fig. 1f displays the X-ray diffraction (XRD) pattern of FA_{0.8}Cs_{0.2}PbI₃ perovskite with different amounts of MACl. FA_{0.8}Cs_{0.2}PbI₃ has two cations, but the molar ratio of FA⁺ is much higher than Cs⁺, so FAPbI₃ plays the main role of a framework, and it contributes to the strongest peak in the XRD pattern. In the trigonal phase of FAPbI₃, the peaks at 14.03° and 28.05° correspond to the (001) and (002) planes [4], respectively, indicating that the black phase was successfully created. There is no signal at 11.8° in the XRD pattern, indicating that the yellow δ-phase of FAPbI₃ was not created during this fabrication. For the polycrystalline thin film, a stronger peak intensity represents a higher crystallinity. The peak intensity is obviously increased upon the incorporation of 4% MACl into the precursor, which means the crystallinity of perovskite is significantly improved by the additive MACl (Fig. 1g). The crystallinity decreased when the amount of MACl is further increased to 10%. The full width at half maximum (FWHM) is inversely correlated with the crystallite size. Fig. 1g shows the decreased FWHM of the (001) plane with the additive of 4% MACl, suggesting a larger crystallite size. When MACl is increased to 10%, the FWHM increases, which indicates that crystallite size is shrank. The results from XRD and SEM are consistent, showing that 4% MACl results

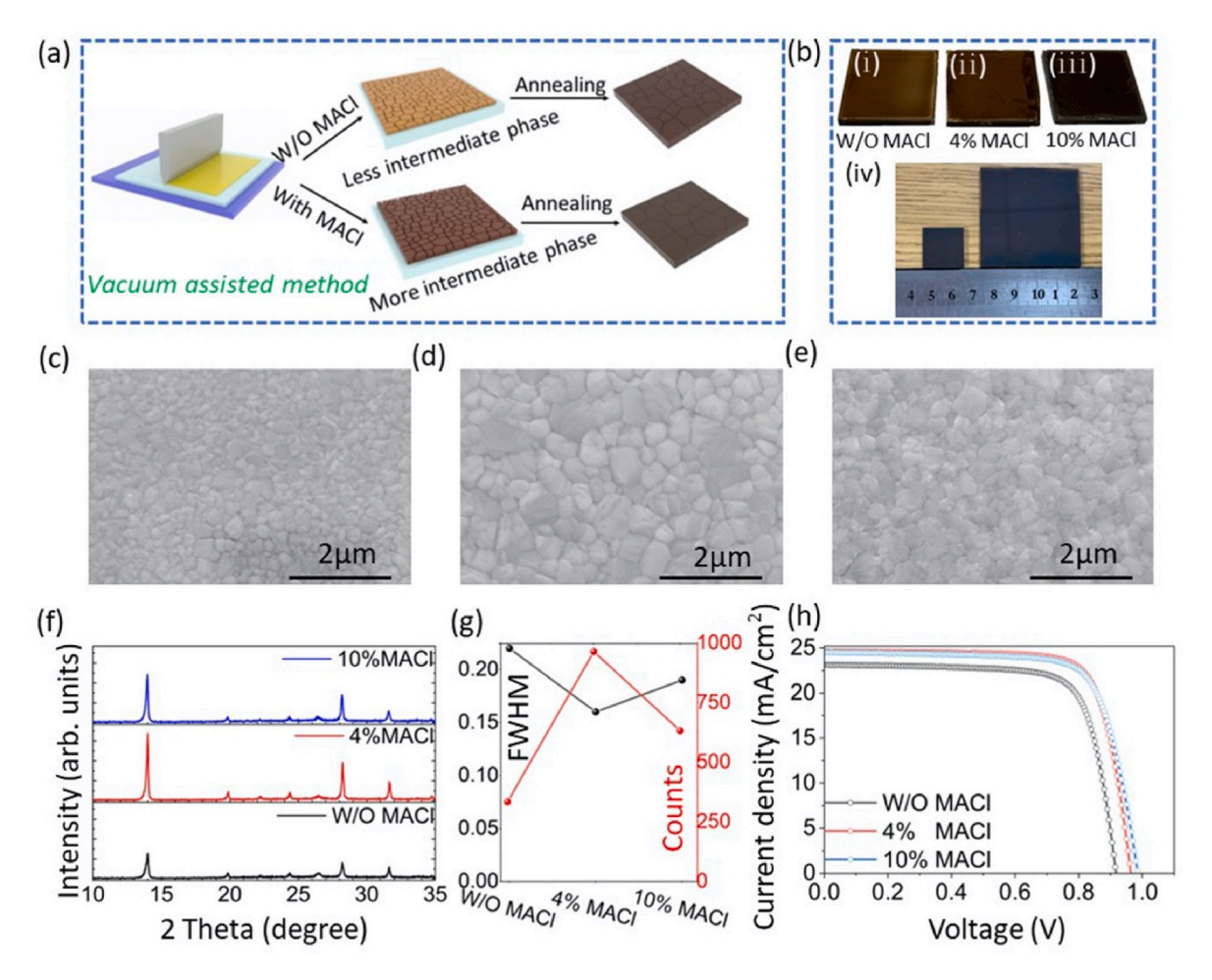


Fig. 1. (a) Schematic illustration of the blade coating followed by vacuum-assisted process and thermal annealing. (b) (i-iii) The photos of the intermediate phase with different amounts of MACl after the vacuum-assisted process. (iv) The photos of blade-coated perovskite films on FTO substrates of two different sizes 2×2 cm² and 5×5 cm² (after thermal annealing). SEM images of FA_{0.8}Cs_{0.2}PbI₃ with (c) no MACl (d) 4% MACl (e) 10% MACl. (f) XRD of FA_{0.8}Cs_{0.2}PbI₃ with different amounts of MACl on FTO substrate (To avoid the influence of extra PbI₂ on XRD, the Pb to AI molar ratio is 0.9:1). (g) The intensity count and FWHM extracted from the XRD pattern. (h) *J-V* characteristics of devices with different amounts of MACl (Pb to AX molar ratio is 1:1).

in better film quality. The absorption edge of UV–vis absorption spectra and steady-state photoluminescence (PL) spectra are most red-shifted with the incorporation of 4% MACl (Fig. S1), since it exhibits the largest crystallinity and crystallite size. The time-resolved PL for the film with 4% MACl also exhibits the longest lifetime (Fig. S1, Table S1). The combination of additive MACl and vacuum assistant method allows us to decouple the nucleation and crystallization process. The existence of MACl slows down the crystallization, while the vacuum removes solvent and drives the nucleation of the wet film. The number of nuclei needs to be suitable. If the solvent evaporation speed is slow, the concentration of the nucleus is low, leaving enough time to grow into large crystals, but resulting in poor coverage. On the other hand, if the solvent evaporation is fast, the time and space for crystal growth are limited. Here, 4% MACl is observed to be the optimum composition.

We fabricated the inverted PSCs with the p-i-n device structure of FTO/NiOx/FA $_{0.8}$ Cs $_{0.2}$ PbI $_3$ /C $_{60}$ /BCP/Cu, since the PSCs with this device structure can be upscalable. Scalable techniques were selected for depositing all layers: hot spray for NiOx, blade coating for perovskite, and thermal evaporation for C60/BCP/Cu. The current density versus voltage (J-V) characteristics and the extracted device parameters of the PSCs with 0%, 4%, and 10% of MACl are shown in Fig. 1h, S1, and summarized in Table S2. The champion PSC without the additive MACl displays a $V_{\rm OC}$ of 0.91 V, a short-circuit current density ($J_{\rm SC}$) of 22.4 mA/cm 2 , a fill factor (FF) of 0.77, and a PCE of 15.7%. The best PSC with 4% MACl shows improved performance, a $V_{\rm OC}$ of 0.96 V, a $J_{\rm SC}$ of 23.6 mA/

cm², a FF of 0.77, resulting in a higher PCE of 17.3%. When the amount of MACl is increased to 10%, the PCE slightly drops. This PCE trend is consistent with the XRD results, a large crystallinity resulting in higher PCE.

2.2. The Pb-A ratio for perovskites on NiOx

Since NiOx can react with AX, producing excess PbI₂ at the interface [53], we varied the Pb-A ratio. XRD pattern (Fig. 2a) of FA_{0.8}Cs_{0.2}PbI₃ with different PbI₂ to AI (A is FA_{0.8}Cs_{0.2}) ratio were collected. When the ratio of PbI2 to AI is 1:1, a peak at 12.7° appears on both fluorine-doped tin oxide (FTO) and NiOx substrates. It suggests that even the molar ratio of A⁺ and Pb²⁺ ions match equally in the perovskite precursor, there is still some left PbI2 that do not participate in the formation of the perovskite phase. In this case, the un-reacted PbI₂ not only suppresses the formation of α -phase but also results in an intrinsic instability of the film under illumination [52]. Once we decrease the amount of PbI₂ by 8%, the PbI₂ peak intensity in the XRD pattern becomes weaker. More importantly, the peak intensity of the (001) plane strongly increases, suggesting that the crystallinity of polycrystalline perovskite film improves significantly. We also found that the peak intensity ratio of PbI2 to the (001) plane is always higher on NiOx substrate than FTO substrate, which means more PbI2 on NiOx than on FTO substrate. This result is due to the $Ni^{\geq 3+}$ sites in NiOx thin films reacting with the organic cation of perovskite, leaving PbI2 on NiOx [53]. Further

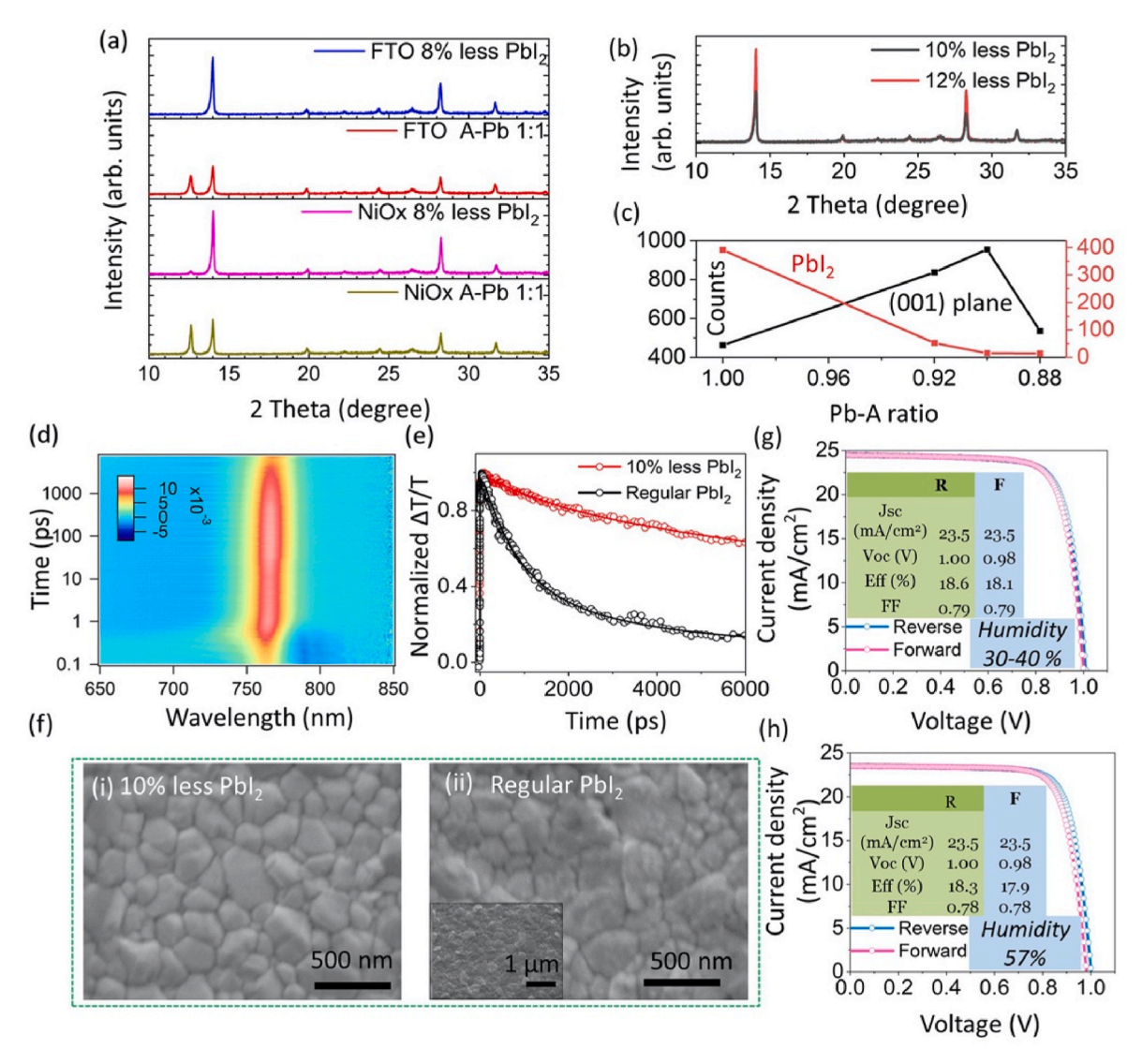


Fig. 2. (a–b) XRD patterns of $FA_{0.8}Cs_{0.2}PbI_3$ perovskites with different PbI_2 to AI ratios on FTO and NiOx substrates. (c) Intensity associated with PbI_2 and (001) peak as a function of Pb-A ratio. (d) Transient absorption spectroscopy of blade-coated $FA_{0.8}Cs_{0.2}PbI_3$ perovskite with 10% less PbI_2 on FTO substrate. (e) Normalized transient absorption kinetics at 764 nm with regular PbI_2 and 10% less PbI_2 . Circles and solid lines represent experimental data and fit, respectively. (f) SEM images of perovskite films with regular PbI_2 and 10% less PbI_2 . J-V characteristics of devices fabricated under humidity (g) 30%–40% RH and (h) 57% RH.

decreasing PbI₂ by 10%, the signal associated with PbI₂ on NiOx substrate in the XRD pattern disappears (Fig. 2b and c), representing that all the PbI₂ participates in the reaction for the perovskite phase. Importantly, the (001) peak intensity is further increased, suggesting enhanced crystallization. Further decreasing PbI₂ from 10% to 12% results in decreased crystallinity (Fig. 2c).

To study the carrier lifetime, we carried out femtosecond laser transient absorption spectroscopy. Fig. 2d displays representative transient absorption spectra of perovskite film. The positive feature at 764 nm corresponds to the ground state bleaching, while the negative feature corresponds to the excited state absorption. Fig. 2e shows extracted kinetics at 764 nm of perovskite films (regular film refers to PbI₂:AI= 1:1, and 10% less PbI₂ refers to PbI₂:AI=0.9:1). By fitting the time traces with multiple exponential decays, we achieved the carrier lifetime of 1 ns (weight ratio 81%) and 6.7 ns (19%) for regular perovskite. The lifetime is increased to 2 ns (20%) and 30 ns (80%), when the amount of PbI₂ is decreased by 10%. The fast decay is due to the nonradiative recombination caused by the traps, while the slow decay is attributed to the radiative recombination of free electrons and holes in perovskite film [54,55]. The longer lifetime arises from the superior film quality, better crystallinity, and reduced trap density. The

scanning electronic microscope (SEM) displays that the grain surface of regular PbI_2 is rough relative to that with 10% less PbI_2 , indicating that unreacted PbI_2 might restrict the smooth crystal growth at the surface (Fig. 2f). The results of XRD, transient absorption, and SEM all suggest that less PbI_2 is crucial to achieving efficient PSCs, in particular on NiOx substrates.

We fabricated PSCs based on the less 10% Pb-A ratio in air with humidity of 30%–57% RH. The best device (30%–40% RH) displays Voc of 1.00 V, J_{SC} of 23.5 mA/cm², FF of 0.79, resulting in a champion PCE of 18.6% (Fig. 2g). The above approach is also applicable to the high humidity environment. We fabricated the same device in air with a humidity of 57%. The champion PCE is 18.3% (Fig. 2h), suggesting that this fabrication method also works in a high humidity environment.

2.3. Light soaking effect

We also found that light soaking with a few hours can further improve the V_{OC} of PSCs. The enhanced Voc could be from two factors: one is the deactivation of defects in the bulk of perovskite, and the other is trap filling or built-in electric field at the interface between NiOx and perovskite [56]. To explore the origin of Voc improvement under

illumination, we studied the light soaking effect on the bulk of perovskite and the NiOx/perovskite interface. XRD experiments were carried out for perovskite films on NiOx with 2-day light soaking and without light soaking (Fig. S2). The XRD pattern is not sensitive to the light soaking time, suggesting that light soaking does not affect the crystallinity of perovskite in the bulk. We carried out transient absorption spectroscopy to quantify the carrier lifetime under light soaking. Fig. 3a displays the transient absorption spectra of perovskite on NiOx without any light soaking. Fig. 3b shows the normalized kinetics at 764 nm of perovskite films with different light soaking times (0h, 2h, 12h). It is clearly observed that with the increase in light soaking time from 0h, 2h, to 12 h, both fast decay and slow decay time components on NiOx substrate increased significantly. By fitting the kinetics, the carrier lifetime is increased from 1 ns (47%) and 5 ns (53%) for 0 h, 1 ns (33%) and 8 ns (67%) for 2 h, to 2 ns (30%) and 42 ns (70%) for 12 h. To further probe whether it is substrate dependent, we carried out transient absorption spectroscopy on perovskite deposited on another substrate FTO where the charge transfer is not significant (Fig. 3c, S3c-d). We found that the carrier lifetime of perovskite on FTO is insensitive to the light soaking (Fig. 3d), suggesting that the light soaking does not affect the bulk property of perovskite, which is consistent with the XRD results. The above results suggest that the enhanced carrier lifetime on NiOx under light soaking is related to NiOx/perovskite interface.

To probe the interface, we applied transient reflection spectroscopy for perovskite films on NiOx before (Fig. 3e) and after light soaking (Fig. S3e), with the laser shining from the substrate side. The probe pulse in transient absorption is transmitted through the entire film, while it is reflected in the geometry of transient reflection. Therefore, the transient reflection technique is more sensitive to the interface [57]. In transient reflection, the negative feature is from the ground state bleaching, while the positive feature is from the excited state absorption. The carrier lifetime measured from transient reflection is typically shorter than that from transient absorption, due to the surface recombination and the carrier diffusion from the surface to the bulk [57]. Similar to transient absorption spectra, transient reflection spectra exhibit a longer lifetime under light soaking. By fitting the kinetics at 770 nm, the carrier lifetime is increased from 0.48 ps (52.4%), 0.17 ns (14.3%), and 4.5 ns (33.3%)

for 0 h light soaking, to 0.85 ps (50.7%), 3.6 ns (17.1%), and 66.7 ns (32.2%) for 18 h light soaking (Fig. 3f). The enhanced carrier lifetime by light soaking could originate from two factors. One possible reason is that the migration of ions can change the built-in electric field, affecting the charge accumulation at the interface [56]. The other is that photogenerated carriers can neutralize the interfacial defects, suppressing the non-radiative recombination at the interface, ultimately improving the $V_{\rm OC}$ [56]. Similar transient reflection experiments were carried out on perovskite film deposited on another substrate FTO, before and after light soaking (Fig. 3g, S3f). Different from the NiOx substrate, the carrier lifetime on the FTO substrate is insensitive to the light soaking (Fig. 3h). Since the charge transfer is much more pronounced at the perovskite/NiOx interface than perovskite/FTO, we suspect that this light soaking effect occurs at the charge transfer interface.

2.4. Device performance

After 6 h of light soaking, the PSCs with the highest PCE of 19.5% (Fig. 4a) were obtained. External quantum efficiency (EQE) and integrated J_{SC} are shown in Fig. 4b. The efficiency extracted from the J-V curve is consistent with that from steady-state measurement (Fig. 4c). Fig. 4d displays the statistical distribution of the PCE of four types of devices (without MACl, with 4% MACl, 10% less PbI2, under 6 h illumination). We found that the higher averaged values were obtained with a small amount of MACl and less PbI2. The best encapsulated device exhibits a good photostability (Fig. 4e) under a whole spectrum of 1 sun light illumination at 45°C and humidity 50%-60% RH. After 648 h of illumination, the PCE maintains 96% of the original value and 91.5% of the maximum value. Table S4 compares the device efficiency and stability with perovskite fabricated by blade coating/slot die and NiOx as the HTL. This work with efficiency 19.5% and photostability T90>648h is among the top. In addition, our method is upscalable for each layer: hot spray for NiOx, blade coating for perovskite, and thermal evaporation for C60/BCP/Cu.

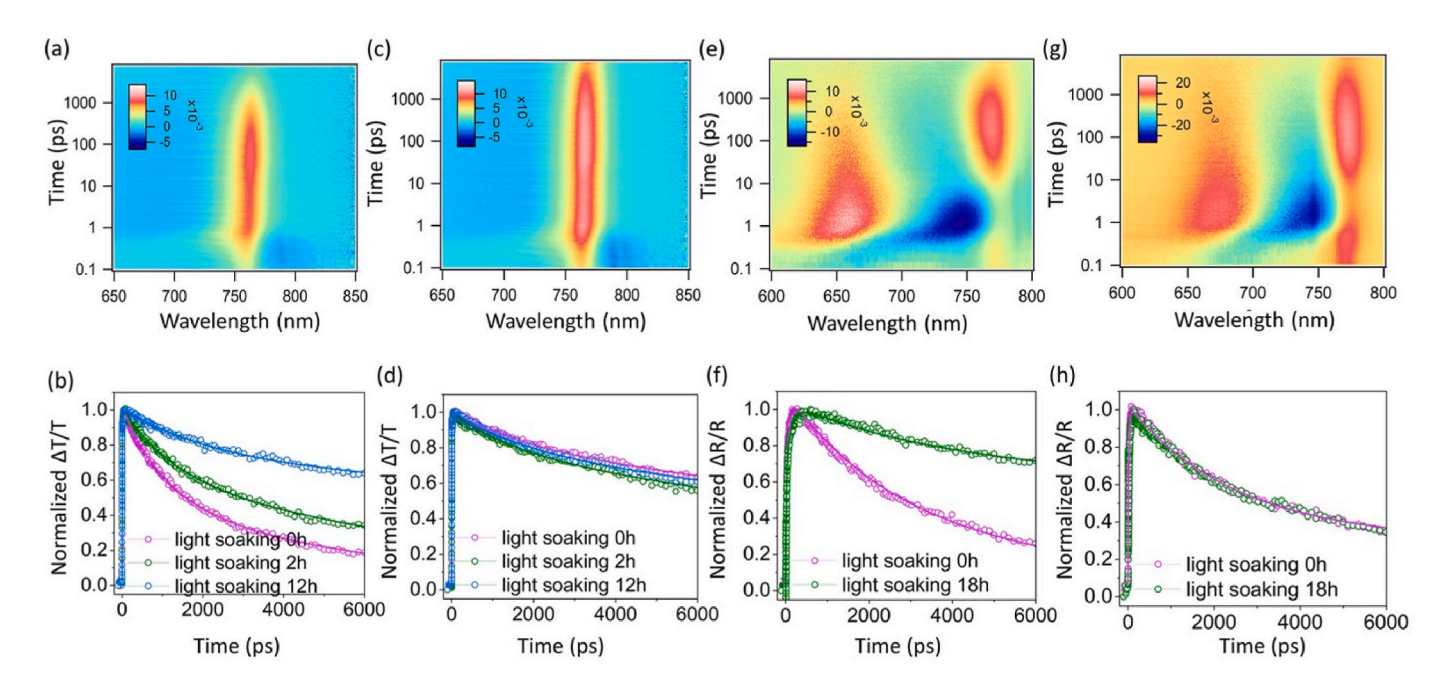


Fig. 3. Transient absorption spectroscopy of $FA_{0.8}Cs_{0.2}PbI_3$ perovskite on (a) NiOx and (c) FTO substrates without light soaking. Normalized transient absorption kinetics of perovskite on (b) NiOx and (d) FTO substrates with 0h, 2h, and 12h light soaking, extracted at 764 nm. Transient reflection spectroscopy of $FA_{0.8}Cs_{0.2}PbI_3$ perovskite on (e) NiOx and (g) FTO substrates without light soaking. Normalized transient reflection kinetics of perovskite on (f) NiOx and (h) FTO substrates with 0h and 18h light soaking, extracted at 770 nm. Circles and solid lines represent experimental data and fit, respectively.

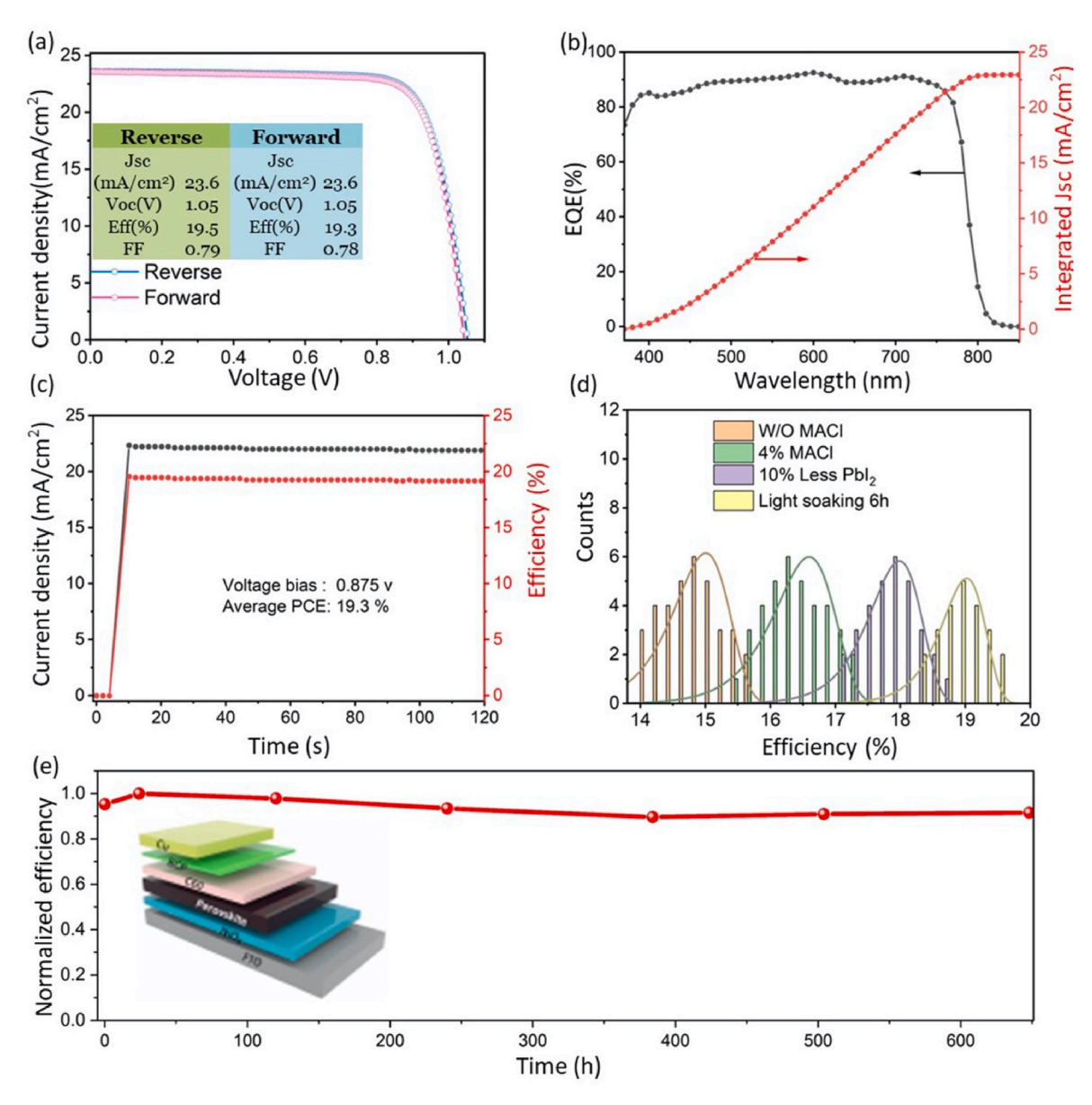


Fig. 4. (a) *J-V* curve of champion FA_{0.8}Cs_{0.2}PbI₃ solar cell. (b) EQE and integrated Jsc. (c) Steady-state current density and PCE. (d) A statistical distribution of the PCE for PSCs. (e) Normalized PCE of photostability test under the illumination of 1 sun at 45°C and 50%–60% RH. Inset is the inverted device architecture (p-i-n) of PSCs.

3. Conclusion

In this work, the blade coating and vacuum-assisted method is applied for inverted FACs-based perovskite solar cells in an ambient environment (30%–57% RH). We investigate the use of the additive MACl in FACsPbI $_3$ perovskite to promote the formation of the intermediate phase during the vacuum quenching process. NiOx is selected as the hole transport material, due to its high photostability, hydrophilic surface, and scalability. Tuning the molar ratio between Pb $^{2+}$ and A $^+$ not only affects the intrinsic property of perovskites but also accommodates the negative effect of the un-reacted PbI $_2$ caused by NiOx. Combined with light soaking, the best vacuum-assisted blade-coated FACsPbI $_3$ device with a PCE of 19.5% was achieved. The encapsulated device exhibits 96% of the original efficiency and 91.5% of the maximum efficiency, after 648 h under the whole spectrum of 1 sun at 45°C and 50%–60% RH. From the perspective of commercialization of PSCs, our work provides a low-cost and scalable approach.

4. Experimental section

Materials: FAI (99.99%) and phenethylammonium chloride (PEACl) were purchased from GreatCell Solar Materials. CsI (99.999%) and nickel (II) 2,4-pentanediaonate (95%) were purchased from Alfa Aesar. PbI₂ (99.99%) was purchased from Tokyo Chemical Industry (TCI). FTO and MACl were purchased from Advanced Election Technology. C60 (99%) was purchased from Nano-C. BCP (99.99%) and all the solvents (anhydrous) were purchased from Millipore Sigma.

Device fabrication and test: FTO is cleaned with detergent, deionized water, alcohol, and acetone sequentially 15 min each using the ultrasonic and dried in an oven at 60 °C for 1 h. The cleaned FTO substrates were treated with UV-Ozone for 15 min to remove organic residues on the surface. Then the FTO substrates were heated on a hot plate with the temperature gradually increased to 450°C. 7.5 mL solution of 4 mg/ml nickel acetylacetonate dissolved in acetonitrile was sprayed on hot FTO substrate to achieve NiOx layer around 20 nm. After spraying, the film was heated at 450°C for another 15 min. After cooling down to room

temperature, the NiOx coated FTO was further treated with UV-ozone for another 3-5 min to completely oxidize NiOx. 0.96 M FAI, 0.24 M CsI, and 1.05-1.2 M PbI2 were dissolved in DMF/NMP (5:1 in volume ratio) solution. 0.3 mg/mL PEACl was added into the precursor to suppress the nonradiative recombination and improve stability [20], and different amounts of MACl (0%, 4%, and 10% in molar ratio relative to Pb) were added. For the substrate 2×2 cm², 5 μ L perovskite precursor was used on NiOx coated FTO substrate for blade coating. The gap between substrate and blade coater was around 150 μm and the coating speed was 3.5 mm/s. This process was completed in air with humidity 30%-57% RH. After the substrate was completely covered by perovskite precursor, the wetting substrate was immediately transferred into a vacuum chamber, which was pumped to a gauge pressure < -1 bar in 10 s and kept for 2 min. The film was annealed at 75°C for 5 min to crystalize the perovskite in a nitrogen-filled glove box and then transferred to an ambient environment where the substrate was annealed at 150°C for 10 min to completely change to black phase. After cooling down to room temperature, 30 nm C60, 10 nm BCP, and 90 nm copper were thermally evaporated at the pressure under 1.5×10^{-6} Torr. The device's active area is 0.10 cm². The *I–V* curves and steady-state power conversion efficiencies were measured by Keithley 2612B source meter with a Xenon solar simulator under AM 1.5G and 100 mW/cm² illumination. The prepared solar cells were encapsulated with cover glass using epoxy AB glue and aged overnight with pressure before the photostability test. The photostability was tested under open circuit at 45°C and 50%–60% RH, a full spectrum metal halide light bulb with an intensity of 100 mW/cm² calibrated by silicon cell [58].

Characterization: SEM image was acquired on a JEOL JSM-7100F scanning electron microscope. XRD experiments were carried out using PANalytical X-ray diffractometer under the step size of 0.01° . The UV-vis linear absorption spectra were obtained by Agilent UV spectrophotometer (Cary 60). The femtosecond transient absorption and reflection were collected using a collinear pump-probe setup (Ultrafast Systems), similar to the previous report [57]. The 400 nm pump was produced by doubling the frequency of Ti:sapphire laser pulse (Coherent Astrella, 800 nm, 5 KHz), while the supercontinuum white light probe was generated by focusing a small part of laser fundamental onto a sapphire. The pump and probe were overlapped onto the sample with the pump-probe time delay controlled by a mechanical delay stage. The cross-correlation between pump and probe was around 100 fs. The external quantum efficiency (EQE) was obtained from the solar cell quantum efficiency measurement system (QEX10) with a 300 W steady-state xenon lamp as the source light.

CRediT authorship contribution statement

Xinwen Zhang: Writing – original draft, Data curation, Conceptualization. Lening Shen: Writing – review & editing, Data curation. Pramod Baral: Writing – review & editing, Data curation. S.N. Vijayaraghavan: Data curation. Feng Yan: Resources, Data curation. Xiong Gong: Writing – review & editing, Supervision, Resources. He Wang: Writing – original draft, Supervision, Resources, Project administration, Funding acquisition, Conceptualization.

Declaration of competing interest

The authors declare that they have no known competing financial interests or personal relationships that could have appeared to influence the work reported in this paper.

Data availability

Data will be made available on request.

Acknowledgments

H. W. acknowledges the financial support by the Air Force Office of Scientific Research (AFOSR) under award number FA9550-17-1-0099 and FA9550-21-1-0192.

Appendix A. Supplementary data

Supplementary data to this article can be found online at https://doi. org/10.1016/j.solmat.2022.111894.

References

- Best research-cell efficiencies. https://www.nrel.gov/pv/assets/pdfs/best-resear ch-cell-efficiencies-rev211214.pdf.
- [2] S.D. Stranks, G.E. Eperon, G. Grancini, C. Menelaou, M.J. Alcocer, T. Leijtens, L. M. Herz, A. Petrozza, H.J. Snaith, Electron-hole diffusion lengths exceeding 1 micrometer in an organometal trihalide perovskite absorber, Science 342 (2013) 341–344, https://doi.org/10.1126/science.1243982.
- [3] Q. Dong, Y. Fang, Y. Shao, P. Mulligan, J. Qiu, L. Cao, J. Huang, Electron-hole diffusion lengths > 175 μm in solution-grown CH₃NH₃PbI₃ single crystals, Science 347 (2015) 967–970, https://doi.org/10.1126/science.aaa5760.
- [4] A.A. Zhumekenov, M.I. Saidaminov, M.A. Haque, E. Alarousu, S.P. Sarmah, B. Murali, I. Dursun, X.-H. Miao, A.L. Abdelhady, T. Wu, O.F. Mohammed, O. M. Bakr, Formamidinium lead halide perovskite crystals with unprecedented long carrier dynamics and diffusion length, ACS Energy Lett. 1 (2016) 32–37, https:// doi.org/10.1021/acsenergylett.6b00002.
- [5] K. Hwang, Y.S. Jung, Y.J. Heo, F.H. Scholes, S.E. Watkins, J. Subbiah, D.J. Jones, D.Y. Kim, D. Vak, Toward large scale roll-to-roll production of fully printed perovskite solar cells, Adv. Mater. 27 (2015) 1241–1247, https://doi.org/10.1002/ adma. 201404598
- [6] D.-N. Jeong, D.-K. Lee, S. Seo, S.Y. Lim, Y. Zhang, H. Shin, H. Cheong, N.-G. Park, Perovskite cluster-containing solution for scalable d-bar coating toward highthroughput perovskite solar cells, ACS Energy Lett. 4 (2019) 1189–1195, https:// doi.org/10.1021/acsenergylett.9b00042.
- [7] Z. Wei, H. Chen, K. Yan, S. Yang, Inkjet printing and instant chemical transformation of a CH₃NH₃Pbl₃/nanocarbon electrode and interface for planar perovskite solar cells, Angew. Chem. Int. Ed. 53 (2014) 13239–13243, https://doi. org/10.1002/ange.201408638.
- [8] N.-G. Park, K. Zhu, Scalable fabrication and coating methods for perovskite solar cells and solar modules, Nat. Rev. Mater. 5 (2020) 333–350, https://doi.org/ 10.1038/s41578-019-0176-2.
- [9] Y.Y. Kim, T.-Y. Yang, R. Suhonen, M. Välimäki, T. Maaninen, A. Kemppainen, N. J. Jeon, J. Seo, Gravure-Printed flexible perovskite solar cells: toward roll-to-roll manufacturing, Adv. Sci. 6 (2019), 1802094, https://doi.org/10.1002/advs/201802004
- [10] Z. Yang, W. Zhang, S. Wu, H. Zhu, Z. Liu, Z. Liu, Z. Jiang, R. Chen, J. Zhou, Q. Lu, Z. Xiao, L. Shi, H. Chen, L.K. Ono, S. Zhang, Y. Zhang, Y. Qi, L. Han, W. Chen, Slot-die coating large-area formamidinium-cesium perovskite film for efficient and stable parallel solar module, Sci. Adv. 7 (2021), eabg3749, https://doi.org/10.1126/sciadv.abg3749.
- [11] M. Du, X. Zhu, L. Wang, H. Wang, J. Feng, X. Jiang, Y. Cao, Y. Sun, L. Duan, Y. Jiao, K. Wang, X. Ren, Z. Yan, S. Pang, S. Liu, High-pressure nitrogen-extraction and effective passivation to attain highest large-area perovskite solar module efficiency, Adv. Mater. 32 (2020), 2004979, https://doi.org/10.1002/adma.202004979.
- [12] J. Li, J. Dagar, O. Shargaieva, M.A. Flatken, H. Köbler, M. Fenske, C. Schultz, B. Stegemann, J. Just, D.M. Többens, A. Abate, R. Munir, E. Unger, 20.8% slot-die coated MAPbl₃ perovskite solar cells by optimal DMSO-content and age of 2-ME based precursor inks, Adv. Energy Mater. 11 (2021), 2003460, https://doi.org/ 10.1002/aenm.202003460.
- [13] T.S. Le, D. Saranin, P. Gostishchev, I. Ermanova, T. Komaricheva, L. Luchnikov, D. Muratov, A. Uvarov, E. Vyacheslavova, I. Mukhin, S. Didenko, D. Kuznetsov, A. Di Carlo, All-slot-die-coated inverted perovskite solar cells in ambient conditions with chlorine additives, Solar RRL (2021), https://doi.org/10.1002/solr.202100807, 2100807.
- [14] Y. Zhong, R. Munir, J. Li, M.-C. Tang, M.R. Niazi, D.-M. Smilgies, K. Zhao, A. Amassian, Blade-coated hybrid perovskite solar cells with efficiency> 17%: an in situ investigation, ACS Energy Lett. 3 (2018) 1078–1085, https://doi.org/ 10.1021/acsenergylett.8b00428.
- [15] Y. Deng, X. Zheng, Y. Bai, Q. Wang, J. Zhao, J. Huang, Surfactant-controlled ink drying enables high-speed deposition of perovskite films for efficient photovoltaic modules, Nat. Energy 3 (2018) 560–566, https://doi.org/10.1038/s41560-018-0153-9.
- [16] Y. Deng, C.H. Van Brackle, X. Dai, J. Zhao, B. Chen, J. Huang, Tailoring solvent coordination for high-speed, room-temperature blading of perovskite photovoltaic films, Sci. Adv. 5 (2019) eaax7537, https://doi.org/10.1126/sciadv.aax7537.
- [17] W.Q. Wu, Z. Yang, P.N. Rudd, Y. Shao, X. Dai, H. Wei, J. Zhao, Y. Fang, Q. Wang, Y. Liu, Y. Deng, X. Xiao, Y. Feng, J. Huang, Bilateral alkylamine for suppressing charge recombination and improving stability in blade-coated perovskite solar cells, Sci. Adv. 5 (2019), eaav8925, https://doi.org/10.1126/sciadv.aav8925.

- [18] S. Chen, X. Xiao, H. Gu, J. Huang, Iodine reduction for reproducible and highperformance perovskite solar cells and modules, Sci. Adv. 7 (2021), https://doi. org/10.1126/sciadv.abe8130 eabe8130.
- [19] K. Liu, Q. Liang, M. Qin, D. Shen, H. Yin, Z. Ren, Y. Zhang, H. Zhang, P.W.K. Fong, Z. Wu, J. Huang, J. Hao, Z. Zheng, S.K. So, C.-S. Lee, X. Lu, G. Li, Zwitterionic-surfactant-assisted room-temperature coating of efficient perovskite solar cells, Joule 4 (2020) 2404–2425, https://doi.org/10.1016/j.joule.2020.09.011.
- [20] W.-Q. Wu, P.N. Rudd, Q. Wang, Z. Yang, J. Huang, Blading phase-pure formamidinium-alloyed perovskites for high-efficiency solar cells with low photovoltage deficit and improved stability, Adv. Mater. 32 (2020), 2000995, https://doi.org/10.1002/adma.202000995.
- [21] N. Li, F. Xu, Z. Qiu, J. Liu, X. Wan, X. Zhu, H. Yu, C. Li, Y. Liu, B. Cao, Sealing the domain boundaries and defects passivation by Poly (acrylic acid) for scalable blading of efficient perovskite solar cells, J. Power Sources 426 (2019) 188–196, https://doi.org/10.1016/j.jpowsour.2019.04.041.
- [22] X. Cao, L. Zhi, Y. Jia, Y. Li, K. Zhao, X. Cui, L. Ci, D. Zhuang, J. Wei, A review of the role of solvents in formation of high-quality solution-processed perovskite films, ACS Appl. Mater. Interfaces 11 (2019) 7639–7654, https://doi.org/10.1021/ acsami.8b16315.
- [23] M.K. Kim, H.S. Lee, S.R. Pae, D.-J. Kim, J.-Y. Lee, I. Gereige, S. Park, B. Shin, Effects of temperature and coating speed on the morphology of solution-sheared halide perovskite thin-films, J. Mater. Chem. 6 (2018) 24911–24919, https://doi.org/ 10.1039/c8ta08565i.
- [24] H. Gao, C. Bao, F. Li, T. Yu, J. Yang, W. Zhu, X. Zhou, G. Fu, Z. Zou, Nucleation and crystal growth of organic-inorganic lead halide perovskites under different relative humidity, ACS Appl. Mater. Interfaces 7 (2015) 9110–9117, https://doi.org/ 10.1021/acsami.5b00895.
- [25] Y. Zhou, M. Yang, W. Wu, A.L. Vasiliev, K. Zhu, N.P. Padture, Room-temperature crystallization of hybrid-perovskite thin films via solvent–solvent extraction for high-performance solar cells, J. Mater. Chem. 3 (2015) 8178–8184, https://doi. org/10.1039/c5ta00477b.
- [26] F.X. Xie, D. Zhang, H. Su, X. Ren, K.S. Wong, M. Gratzel, W.C. Choy, Vacuum-assisted thermal annealing of CH₃NH₃PbI₃ for highly stable and efficient perovskite solar cells, ACS Nano 9 (2015) 639–646, https://doi.org/10.1021/nn505978r.
- [27] L. Zeng, S. Chen, K. Forberich, C.J. Brabec, Y. Mai, F. Guo, Controlling the crystallization dynamics of photovoltaic perovskite layers on larger-area coatings, Energy Environ. Sci. 13 (2020) 4666–4690, https://doi.org/10.1039/d0ee02575e.
- [28] J. Li, R. Munir, Y. Fan, T. Niu, Y. Liu, Y. Zhong, Z. Yang, Y. Tian, B. Liu, J. Sun, D.-M. Smilgies, S. Thoroddsen, A. Amassian, K. Zhao, S. Liu, Phase transition control for high-performance blade-coated perovskite solar cells, Joule 2 (2018) 1313–1330, https://doi.org/10.1016/j.joule.2018.04.011.
- [29] S.-H. Turren-Cruz, A. Hagfeldt, M. Saliba, Methylammonium-free, high-performance, and stable perovskite solar cells on a planar architecture, Science 362 (2018) 449–453, https://doi.org/10.1126/science.aat3583.
- [30] Y. Jo, K.S. Oh, M. Kim, K.H. Kim, H. Lee, C.W. Lee, D.S. Kim, High performance of planar perovskite solar cells produced from Pbl₂ (DMSO) and Pbl₂ (NMP) complexes by intramolecular exchange, Adv. Mater. Interfac. 3 (2016), 1500768, https://doi.org/10.1002/admi.201500768
- [31] J.-W. Lee, Z. Dai, C. Lee, H.M. Lee, T.-H. Han, N. De Marco, O. Lin, C.S. Choi, B. Dunn, J. Koh, Tuning molecular interactions for highly reproducible and efficient formamidinium perovskite solar cells via adduct approach, J. Am. Chem. Soc. 140 (2018) 6317–6324, https://doi.org/10.1021/jacs.8b01037.
- [32] F. Yang, L. Dong, D. Jang, K.C. Tam, K. Zhang, N. Li, F. Guo, C. Li, C. Arrive, M. Bertrand, Fully solution processed pure α-phase formamidinium lead iodide perovskite solar cells for scalable production in ambient condition, Adv. Energy Mater. 10 (2020). 2001869. https://doi.org/10.1002/aepm.202001869.
- Mater. 10 (2020), 2001869, https://doi.org/10.1002/aenm.202001869.
 [33] L.-L. Gao, C.-X. Li, C.-J. Li, G.-J. Yang, Large-area high-efficiency perovskite solar cells based on perovskite films dried by the multi-flow air knife method in air, J. Mater. Chem. 5 (2017) 1548–1557, https://doi.org/10.1039/c6ta09565h.
- [34] G. Cotella, J. Baker, D. Worsley, F. De Rossi, C. Pleydell-Pearce, M. Carnie, T. Watson, One-step deposition by slot-die coating of mixed lead halide perovskite for photovoltaic applications, Sol. Energy Mater. Sol. Cells 159 (2017) 362–369, https://doi.org/10.1016/j.solmat.2016.09.013.
- [35] X. Li, D. Bi, C. Yi, J.-D. Décoppet, J. Luo, S.M. Zakeeruddin, A. Hagfeldt, M. Grätzel, A vacuum flash-assisted solution process for high-efficiency large-area perovskite solar cells, Science 353 (2016) 58–62, https://doi.org/10.1126/science.aaf8060.
- [36] K. Choi, H. Choi, J. Min, T. Kim, D. Kim, S.Y. Son, G.-W. Kim, J. Choi, T. Park, A short review on interface engineering of perovskite solar cells: a self-assembled monolayer and its roles, Solar RRL 4 (2020), 1900251, https://doi.org/10.1002/ solr 202070021
- [37] N.J. Jeon, J.H. Noh, W.S. Yang, Y.C. Kim, S. Ryu, J. Seo, S.I. Seok, Compositional engineering of perovskite materials for high-performance solar cells, Nature 517 (2015) 476–480, https://doi.org/10.1038/nature14133.
- [38] Y. Li, L. Ji, R. Liu, C. Zhang, C.H. Mak, X. Zou, H.-H. Shen, S.-Y. Leu, H.-Y. Hsu, A review on morphology engineering for highly efficient and stable hybrid perovskite solar cells, J. Mater. Chem. 6 (2018) 12842–12875, https://doi.org/ 10.1039/C8TA04120B.
- [39] M. Kim, G.-H. Kim, T.K. Lee, I.W. Choi, H.W. Choi, Y. Jo, Y.J. Yoon, J.W. Kim, J. Lee, D. Huh, H. Lee, S.K. Kwak, J.Y. Kim, D.S. Kim, Methylammonium chloride induces intermediate phase stabilization for efficient perovskite solar cells, Joule 3 (2019) 2179–2192, https://doi.org/10.1016/j.joule.2019.06.014.

- [40] Y. Zhao, K. Zhu, CH₃NH₃Cl-assisted one-step solution growth of CH₃NH₃PbI₃: structure, charge-carrier dynamics, and photovoltaic properties of perovskite solar cells, J. Phys. Chem. C 118 (2014) 9412–9418, https://doi.org/10.1021/ ip502606w
- [41] I.S. Yang, N.G. Park, Dual additive for simultaneous improvement of photovoltaic performance and stability of perovskite solar cell, Adv. Funct. Mater. 31 (2021), 2100396, https://doi.org/10.1002/adfm.202100396.
- [42] D. Di Girolamo, F. Di Giacomo, F. Matteocci, A.G. Marrani, D. Dini, A. Abate, Progress, highlights and perspectives on NiO in perovskite photovoltaics, Chem. Sci. 11 (2020) 7746–7759, https://doi.org/10.1039/d0sc02859b.
- [43] X. Yin, P. Chen, M. Que, Y. Xing, W. Que, C. Niu, J. Shao, Highly efficient flexible perovskite solar cells using solution-derived NiOx hole contacts, ACS Nano 10 (2016) 3630–3636, https://doi.org/10.1021/acsnano.5b08135.
- [44] Z. Zhu, Y. Bai, T. Zhang, Z. Liu, X. Long, Z. Wei, Z. Wang, L. Zhang, J. Wang, F. Yan, S. Yang, High-performance hole-extraction layer of sol-gel-processed NiO nanocrystals for inverted planar perovskite solar cells, Angew. Chem. Int. Ed. 53 (2014) 12571–12575, https://doi.org/10.1002/ange.201405176.
- [45] W. Chen, Y. Wu, Y. Yue, J. Liu, W. Zhang, X. Yang, H. Chen, E. Bi, I. Ashraful, M. Gratzel, L. Han, Efficient and stable large-area perovskite solar cells with inorganic charge extraction layers, Science 350 (2015) 944–948, https://doi.org/10.1126/science.aad1015.
- [46] D. Koushik, M. Jošt, A. Dučinskas, C. Burgess, V. Zardetto, C. Weijtens, M. A. Verheijen, W.M. Kessels, S. Albrecht, M. Creatore, Plasma-assisted atomic layer deposition of nickel oxide as hole transport layer for hybrid perovskite solar cells, J. Mater. Chem. C 7 (2019) 12532–12543, https://doi.org/10.1039/c9tc04282b.
- [47] G. Li, Y. Jiang, S. Deng, A. Tam, P. Xu, M. Wong, H.S. Kwok, Overcoming the limitations of sputtered nickel oxide for high-efficiency and large-area perovskite solar cells, Adv. Sci. 4 (2017), 1700463, https://doi.org/10.1002/ advs.201700463
- [48] B. Zhang, J. Su, X. Guo, L. Zhou, Z. Lin, L. Feng, J. Zhang, J. Chang, Y. Hao, NiO/Perovskite heterojunction contact engineering for highly efficient and stable perovskite solar cells, Adv. Sci. 7 (2020), 1903044, https://doi.org/10.1002/pdf. 201903044
- [49] Z. Qiu, H. Gong, G. Zheng, S. Yuan, H. Zhang, X. Zhu, H. Zhou, B. Cao, Enhanced physical properties of pulsed laser deposited NiO films via annealing and lithium doping for improving perovskite solar cell efficiency, J. Mater. Chem. C 5 (2017) 7084–7094, https://doi.org/10.1039/C7TC01224A.
- [50] X. Wan, Y. Jiang, Z. Qiu, H. Zhang, X. Zhu, I. Sikandar, X. Liu, X. Chen, B. Cao, Zinc as a new dopant for NiO x-based planar perovskite solar cells with stable efficiency near 20, ACS Appl. Energy Mater. 1 (2018) 3947–3954, https://doi.org/10.1021/ acsaem.8b00671.
- [51] W. Chen, Y. Zhou, G. Chen, Y. Wu, B. Tu, F.Z. Liu, L. Huang, A.M.C. Ng, A. B. Djurišić, Z. He, Alkali chlorides for the suppression of the interfacial recombination in inverted planar perovskite solar cells, Adv. Energy Mater. 9 (2019), 1803872, https://doi.org/10.1002/aenm.201970068.
 [52] Y. Deng, S. Xu, S. Chen, X. Xiao, J. Zhao, J. Huang, Defect compensation in
- [52] Y. Deng, S. Xu, S. Chen, X. Xiao, J. Zhao, J. Huang, Defect compensation in formamidinium-caesium perovskites for highly efficient solar mini-modules with improved photostability, Nat. Energy 6 (2021) 633–641, https://doi.org/10.1038/ s41560-021-00831-8.
- [53] C.C. Boyd, R.C. Shallcross, T. Moot, R. Kerner, L. Bertoluzzi, A. Onno, S. Kavadiya, C. Chosy, E.J. Wolf, J. Werner, J.A. Raiford, C.d. Paula, A.F. Palmstrom, Z.J. Yu, J. J. Berry, S.F. Bent, Z.C. Holman, J.M. Luther, M.D. McGehee, Overcoming redox reactions at perovskite-nickel oxide interfaces to boost voltages in perovskite solar cells, Joule 4 (2020) 1759–1775, https://doi.org/10.1016/j.joule.2020.06.004.
- [54] X. Ren, B. Zhang, L. Zhang, J. Wen, B. Che, D. Bai, J. You, T. Chen, S. Liu, Deep-level transient spectroscopy for effective passivator selection in perovskite solar cells to attain high efficiency over 23, ChemSusChem 14 (2021) 3182–3189, https://doi.org/10.1002/cssc.202100980.
- [55] L. Wang, C. McCleese, A. Kovalsky, Y. Zhao, C. Burda, Femtosecond time-resolved transient absorption spectroscopy of CH₃NH₃PbI₃ perovskite films: evidence for passivation effect of PbI₂, J. Am. Chem. Soc. 136 (2014) 12205–12208, https://doi. org/10.1021/j.59046329.
- [56] C. Zhao, B. Chen, X. Qiao, L. Luan, K. Lu, B. Hu, Revealing underlying processes involved in light soaking effects and hysteresis phenomena in perovskite solar cells, Adv. Energy Mater. 5 (2015), 1500279, https://doi.org/10.1002/ aenm.201500279.
- [57] M. Zhou, J.S. Sarmiento, C. Fei, H. Wang, Charge transfer and diffusion at the perovskite/PCBM interface probed by transient absorption and reflection, J. Phys. Chem. C 123 (2019) 22095–22103, https://doi.org/10.1021/acs.jpcc.9b07591.
- [58] M.V. Khenkin, E.A. Katz, A. Abate, G. Bardizza, J.J. Berry, C. Brabec, F. Brunetti, V. Bulović, Q. Burlingame, A. Di Carlo, R. Cheacharoen, Y.-B. Cheng, A. Colsmann, S. Cros, K. Domanski, M. Dusza, C.J. Fell, S.R. Forrest, Y. Galagan, D. Di Girolamo, M. Grätzel, A. Hagfeldt, E. von Hauff, H. Hoppe, J. Kettle, H. Köbler, M.S. Leite, S. Liu, Y.-L. Loo, J.M. Luther, C.-Q. Ma, M. Madsen, M. Manceau, M. Matheron, M. McGehee, R. Meitzner, M.K. Nazeeruddin, A.F. Nogueira, Ç. Odabaşı, A. Osherov, N.-G. Park, M.O. Reese, F. De Rossi, M. Saliba, U.S. Schubert, H. J. Snaith, S.D. Stranks, W. Tress, P.A. Troshin, V. Turkovic, S. Veenstra, I. Visoly-Fisher, A. Walsh, T. Watson, H. Xie, R. Yıldırım, S.M. Zakeeruddin, K. Zhu, M. Lira-Cantu, Consensus statement for stability assessment and reporting for perovskite photovoltaics based on ISOS procedures, Nat. Energy 5 (2020) 35–49, https://doi.org/10.1038/s41560-019-0529-5.